Supplemental information

Assessment of optimized FRET substrates as universal corona- and picornavirus main protease substrates for screening assays

Conrad Fischer,[a] Tayla J. Van Oers,[a] Marco J. van Belkum,[a] Tess Lamer,[a] Aaron Romney,[a] Pu Chen,[b] M. Joanne Lemieux[b] and John C. Vederas[a,*]

[a] Department of Chemistry, University of Alberta, Edmonton AB, T6G 2G2, Canada

[b] Department of Biochemistry, Membrane Protein Disease Research Group, University of Alberta, Edmonton AB, T6G 2R3, Canada

* correspondence author email: john.vederas@ualberta.ca

```
FIPV            SGLRKMAQPSGVVEPCIVRVAYGNNVLNGLWLGDEVICPRHVIASDTS-RVINYENELSS  59
PEDV            AGLRKMAQPSGVVEKCIVRVCYGNMALNGLWLGDTVMCPRHVIASSTT-STIDYDYALSV  59
SARS-CoV-2      SGFRKMAFPSGKVEGCMVQVTCGTTTLNGLWLDDVVYCPRHVICTSEDMLNPNYEDLLIR  60
EqCoV           SGIVKMVNPTSKVEPCIVSVTYGNMTLNGLWLDDKVYCPRHVICSASDMTNPDYTNLLCR  60
                :*: **. *:. ** *:* *  *. .******.* * ******.:       :*   *

FIPV            VRLHNFSIAKNNVFLGVVSAKYKGVNLVLKVNQVNPNTPEHKFKSVRPGESFNILACYEG  119
PEDV            LRLHNFSISSGNVFLGVVGVTMRGALLQIKVNQNNVHTPKYTYRTVRPGESFNILACYDG  119
SARS-CoV-2      KSNHNFLVQAGNVQLRVIGHSMQNCVLKLKVDTANPKTPKYKFVRIQPGQTFSVLACYNG  120
EqCoV           VTSSDFTVLFDRLSLTVMSYQMQGCMLVLTVTLQNSRTPKYTFGVVKPGETFTVLAAYNG  120
                    :* :  ..: * *:.   :.  * :.*   * .**::.:  ::**::*.:**.*:*

FIPV            CPGSVYGVNMRSQGTIKGSFIAGTCGSVGYVLENGTLYFVYMHHLELGNGSHVGSNLEGE  179
PEDV            AAAGVYGVNMRSNYTIRGSFINGACGSPGYNINNGTVEFCYLHQLELGSGCHVGSDLDGV  179
SARS-CoV-2      SPSGVYQCAMRPNFTIKGSFLNGSCGSVGFNIDYDCVSFCYMHHMELPTGVHAGTDLEGN  180
EqCoV           KPQGAFHVTMRSSYTIKGSFLCGSCGSVGYVLMGDCVKFVYMHQLELSTGCHTGTDFNGD  180
                   ..:   ** . **:***: *:*** *: :  . : * *:*::** .* *.*::::*

FIPV            MYGGYEDQPSMQLEGTNVMSSDNVVAFLYAALINGERWFVTNTSMTLESYNSWAKTNSFT  239
PEDV            MYGGYEDQPTLQVEGASSLFTENVLAFLYAALINGSTWWLSSSRIAVDRFNEWAVHNGMT  239
SARS-CoV-2      FYGPFVDRQTAQAAGTDTTITVNVLAWLYAAVINGDRWFLNRFTTTLNDFNLVAMKYNYE  240
EqCoV           FYGPYKDAQVVQLPVQDYIQSVNFVAWLYAAILNNCNWFVQSDKCSVEDFNVWALSNGFS  240
                :** : *    *    .   : *.:*:****::*.  *::     ::: :*  *   .

FIPV            EIVST--DAFNMLAAKTGYSVEKLLECI-VRLNKGFGGRTILSYGSLCDEFTPIEVIRQM  296
PEDV            TVVNT--DCFSILAAKTGVDVQRLLASI-QSLHKNFGGKQILGYTSLTDEFTTGEVIRQM  296
SARS-CoV-2      PLTQDHVDILGPLSAQTGIAVLDMCASLKELLQNGMNGRTILGSALLEDEFTPFDVVRQC  300
EqCoV           QVKSDLV--IDALASMTGVSLETLLAAI-KRLKNGFQGRQIMGSCSFEDELTPSDVYQQL  297
                 : .     :. *:: **  :  :  .:   *::.: *: *:.   : **:*  :* :*

FIPV            YGVNLQ  302
PEDV            YGVNLQ  302
SARS-CoV-2      SGVTFQ  306
EqCoV           AGIKLQ  303
                 *:.:*
```

Figure S1. Sequence alignment of coronavirus main proteases under investigation. The catalytic dyad (His41, Cys145) is highlighted in green, conserved sub-pocket residues (S1', S1 and S2) important for substrate recognition are highlighted in light grey.

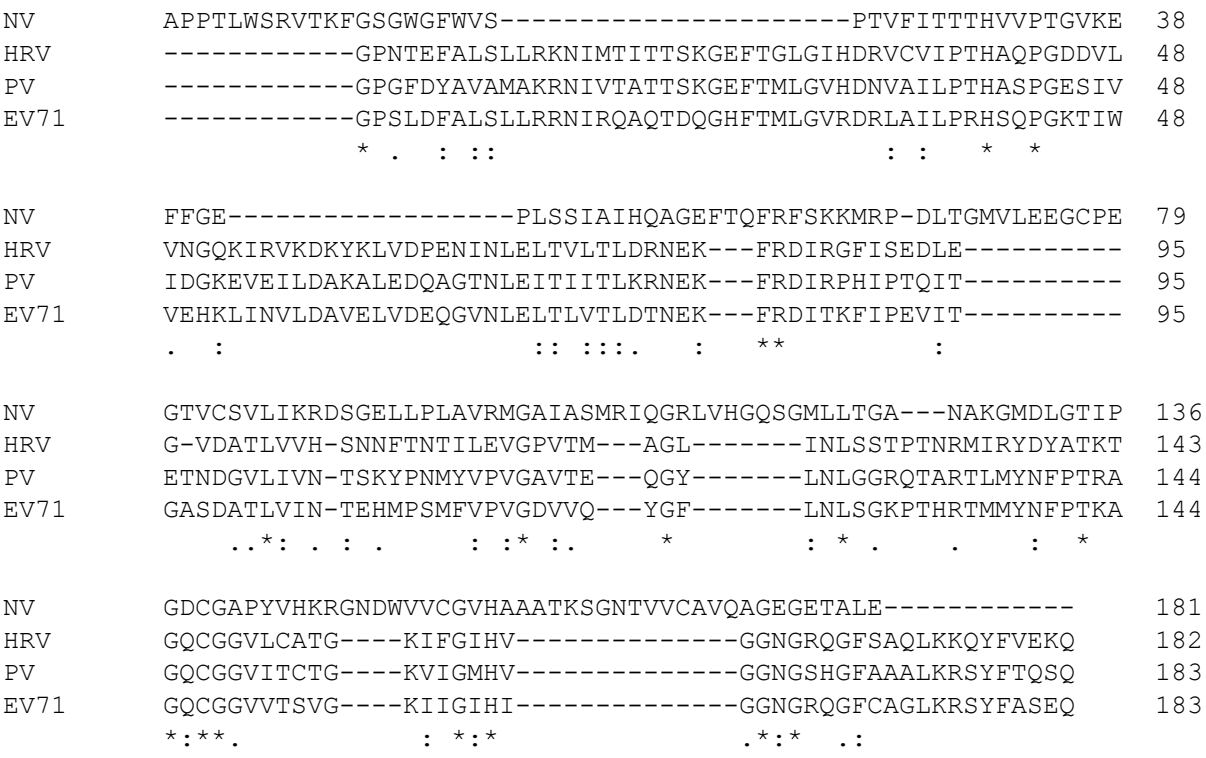

Figure S2. Sequence alignment of picornavirus and norovirus main proteases under investigation. The catalytic triad (His41, Cys147) is highlighted in green, conserved sub-pocket residues (S1', S1 and S2) important for substrate recognition are highlighted in light grey.

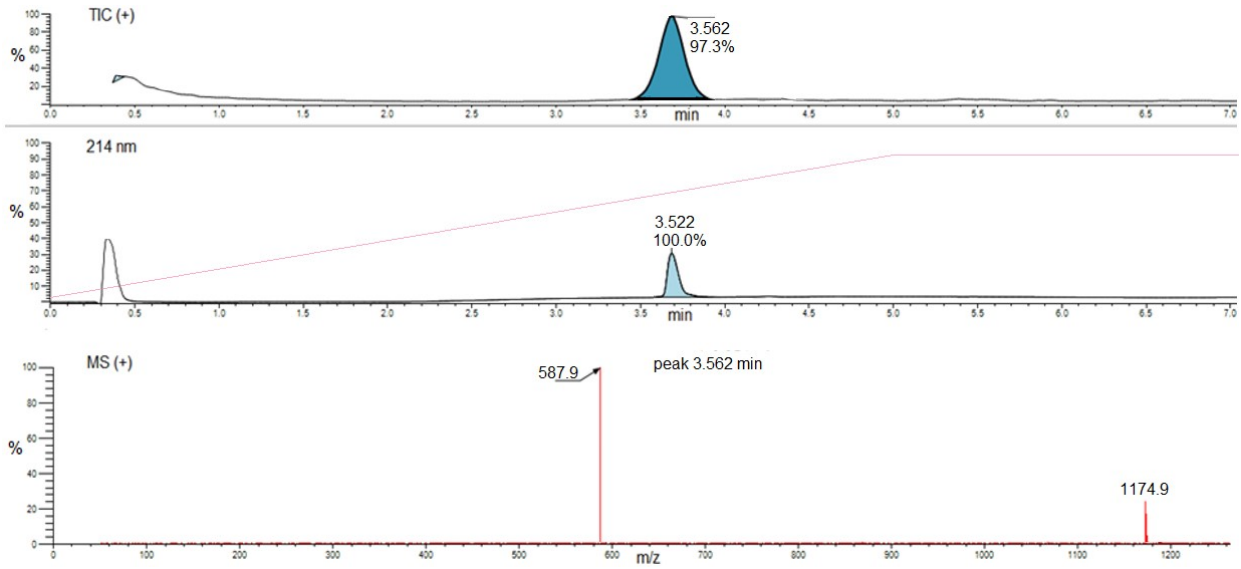

Figure S3. Total ion count chromatogram (TIC+) and mass spectral data for compound **Blanchard** after cleavage of the assembled peptide from SPPS resin and HPLC purification. The solvent gradient (%B = acetonitrile) is highlighted in pink in the DAD chromatogram at 214nm.

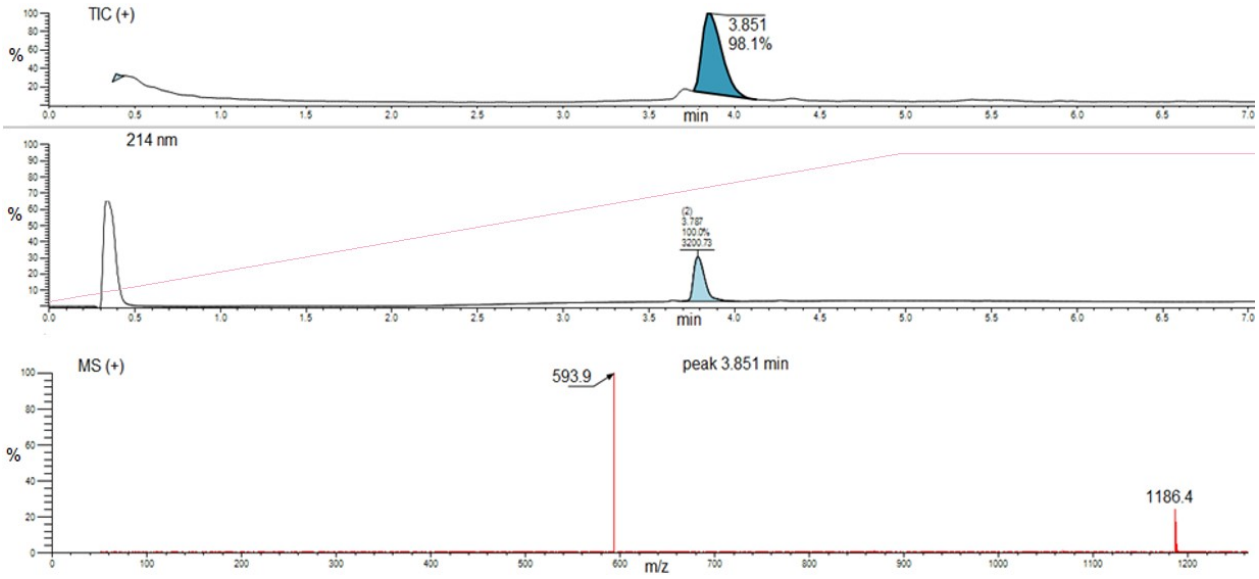

Figure S4. Total ion count chromatogram (TIC+) and mass spectral data for compound **Blanchard-VV** after cleavage of the assembled peptide from SPPS resin and HPLC purification. The solvent gradient (%B = acetonitrile) is highlighted in pink in the DAD chromatogram at 214nm.

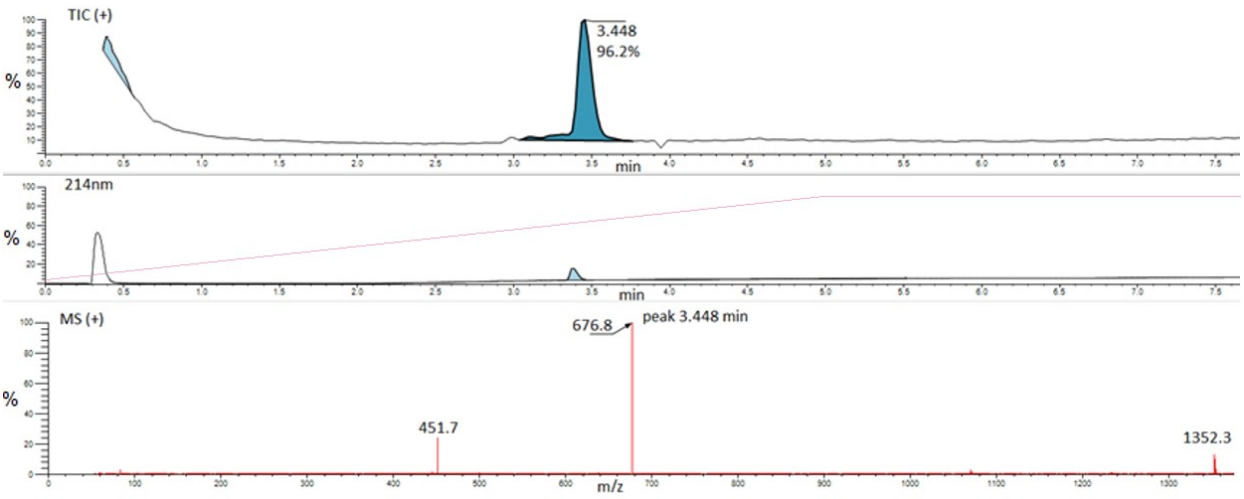

Figure S5. Total ion count chromatogram (TIC+) and mass spectral data for compound **PEDV 1** after cleavage of the assembled peptide from SPPS resin and HPLC purification. The solvent gradient (%B = acetonitrile) is highlighted in pink in the DAD chromatogram at 214nm.

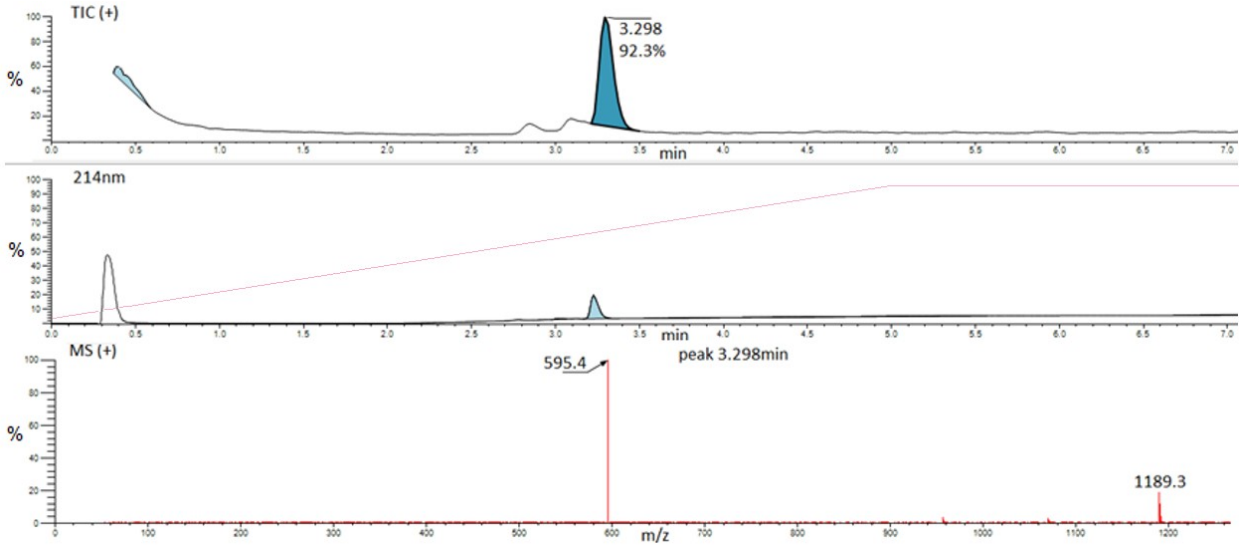

Figure S6. Total ion count chromatogram (TIC+) and mass spectral data for compound **PEDV 2** after cleavage of the assembled peptide from SPPS resin and HPLC purification. The solvent gradient (%B = acetonitrile) is highlighted in pink in the DAD chromatogram at 214nm.

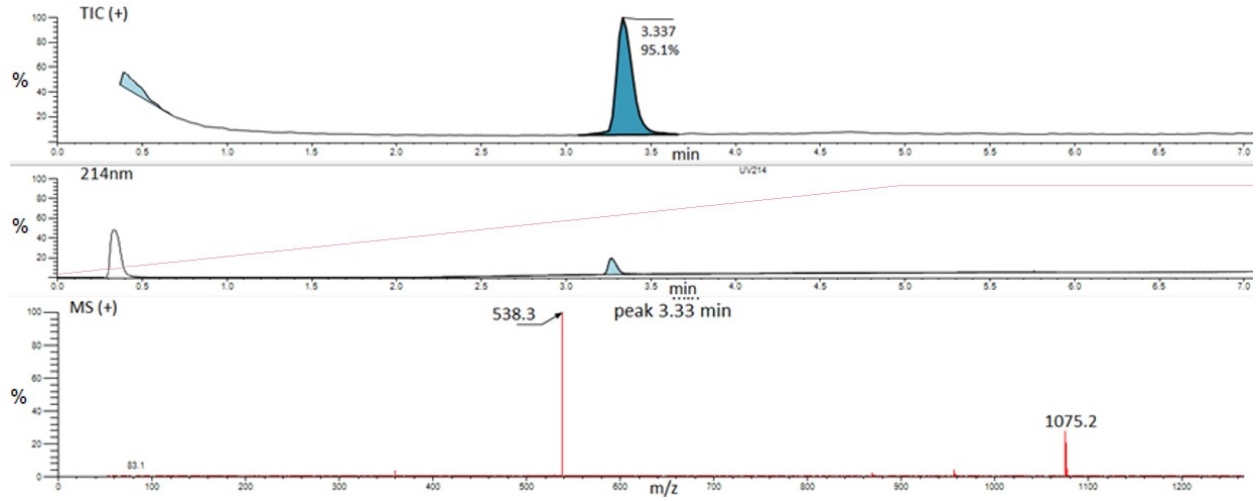

Figure S7. Total ion count chromatogram (TIC+) and mass spectral data for compound **PEDV 3** after cleavage of the assembled peptide from SPPS resin and HPLC purification. The solvent gradient (%B = acetonitrile) is highlighted in pink in the DAD chromatogram at 214nm.

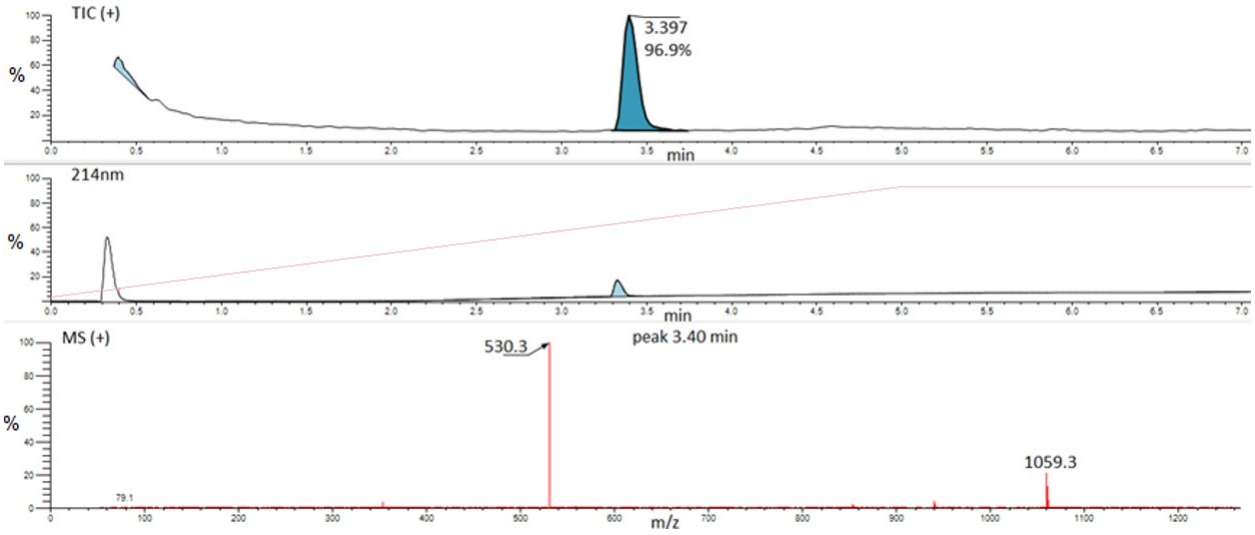

Figure S8. Total ion count chromatogram (TIC+) and mass spectral data for compound **PEDV 4** after cleavage of the assembled peptide from SPPS resin and HPLC purification. The solvent gradient (%B = acetonitrile) is highlighted in pink in the DAD chromatogram at 214nm.

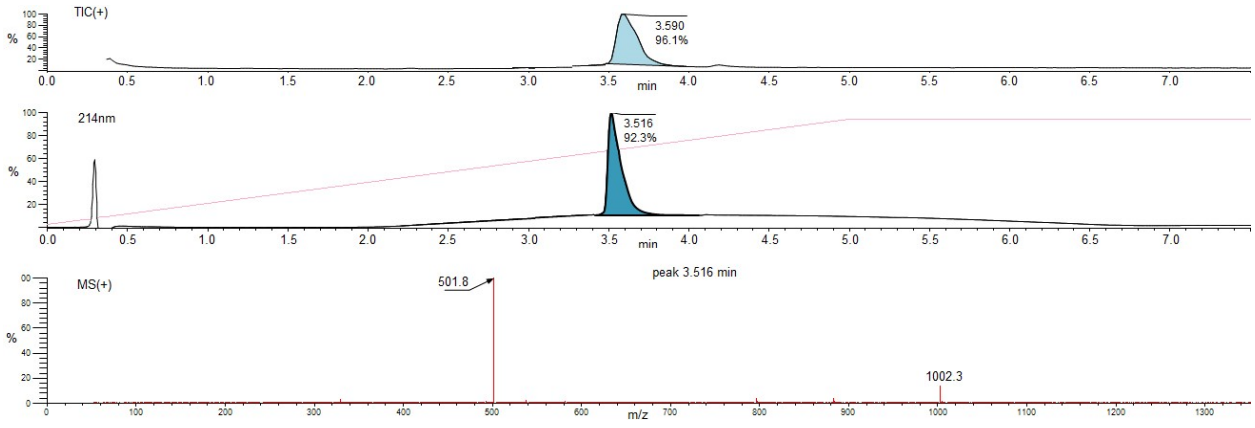

Figure S9. Total ion count chromatogram (TIC+) and mass spectral data for compound **(-)FRET** (negative control) after cleavage of the assembled peptide from SPPS resin and HPLC purification. The solvent gradient (%B = acetonitrile) is highlighted in pink in the DAD chromatogram at 214nm.

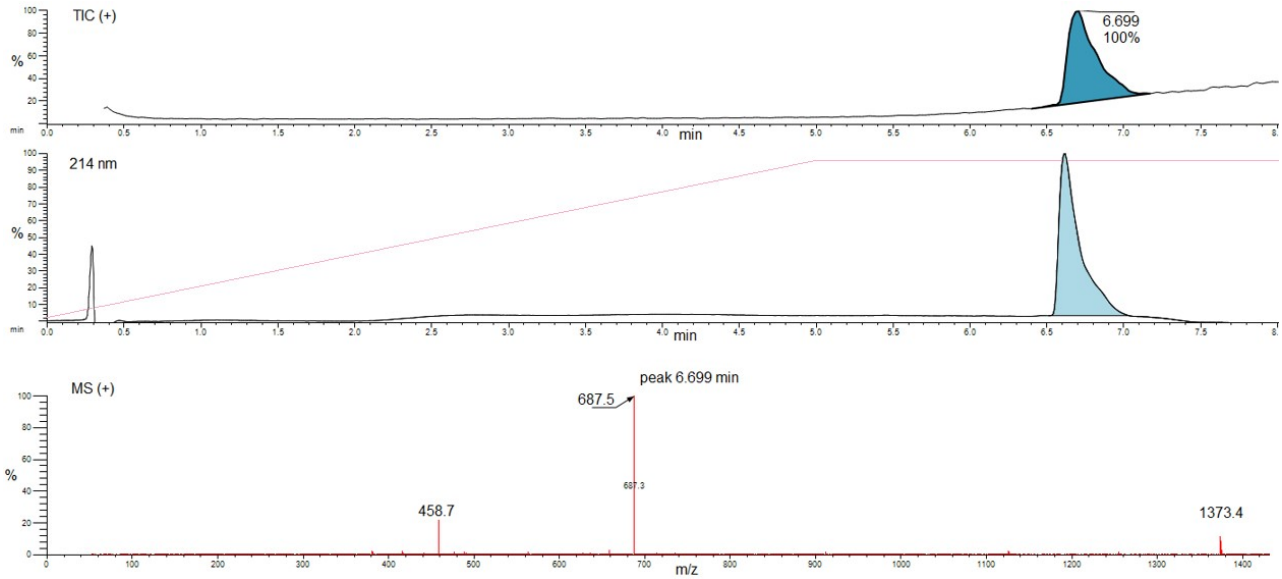

Figure S10. Total ion count chromatogram (TIC+) and mass spectral data for compound **HRVFRET** after cleavage of the assembled peptide from SPPS resin and HPLC purification. The solvent gradient (%B = acetonitrile) is highlighted in pink in the DAD chromatogram at 214nm.

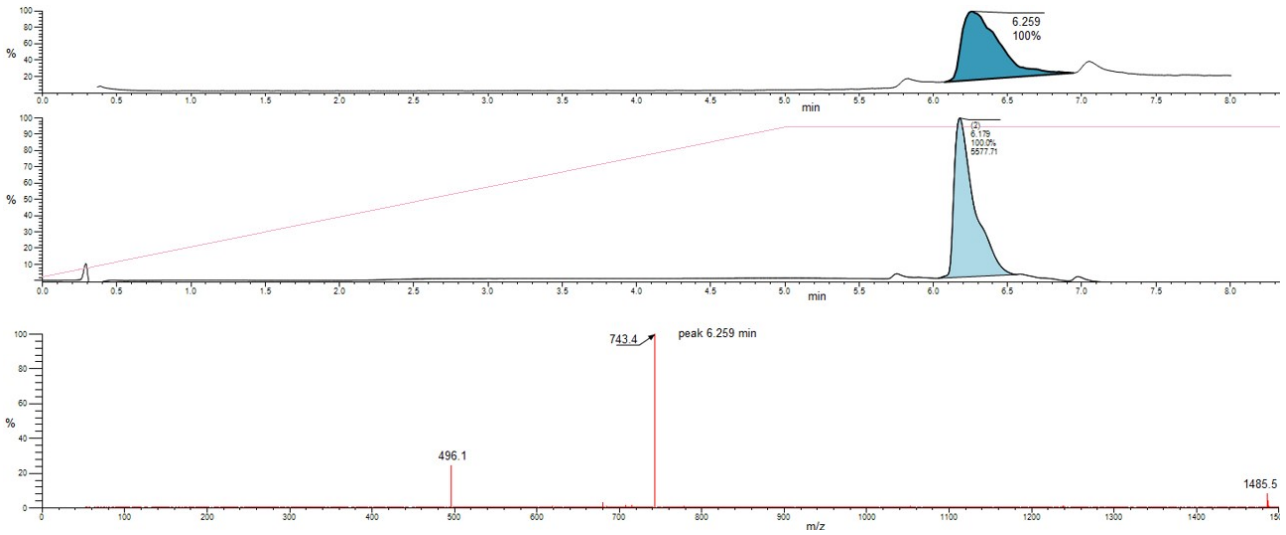

Figure S11. Total ion count chromatogram (TIC+) and mass spectral data for compound **PVFRET** after cleavage of the assembled peptide from SPPS resin and HPLC purification. The solvent gradient (%B = acetonitrile) is highlighted in pink in the DAD chromatogram at 214nm.

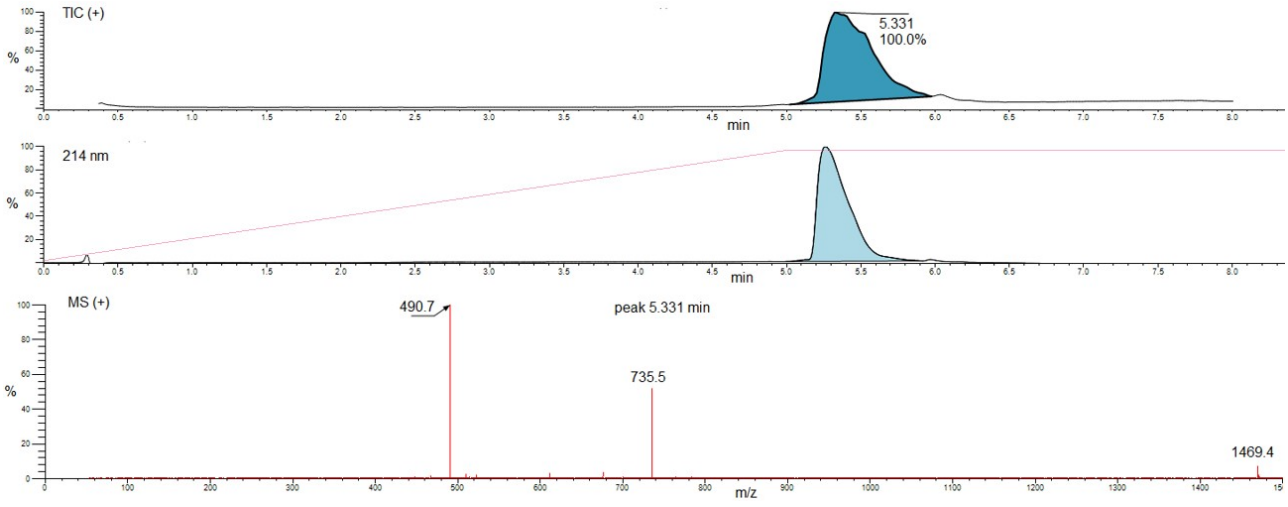

Figure S12. Total ion count chromatogram (TIC+) and mass spectral data for compound **EVFRET** after cleavage of the assembled peptide from SPPS resin and HPLC purification. The solvent gradient (%B = acetonitrile) is highlighted in pink in the DAD chromatogram at 214nm.

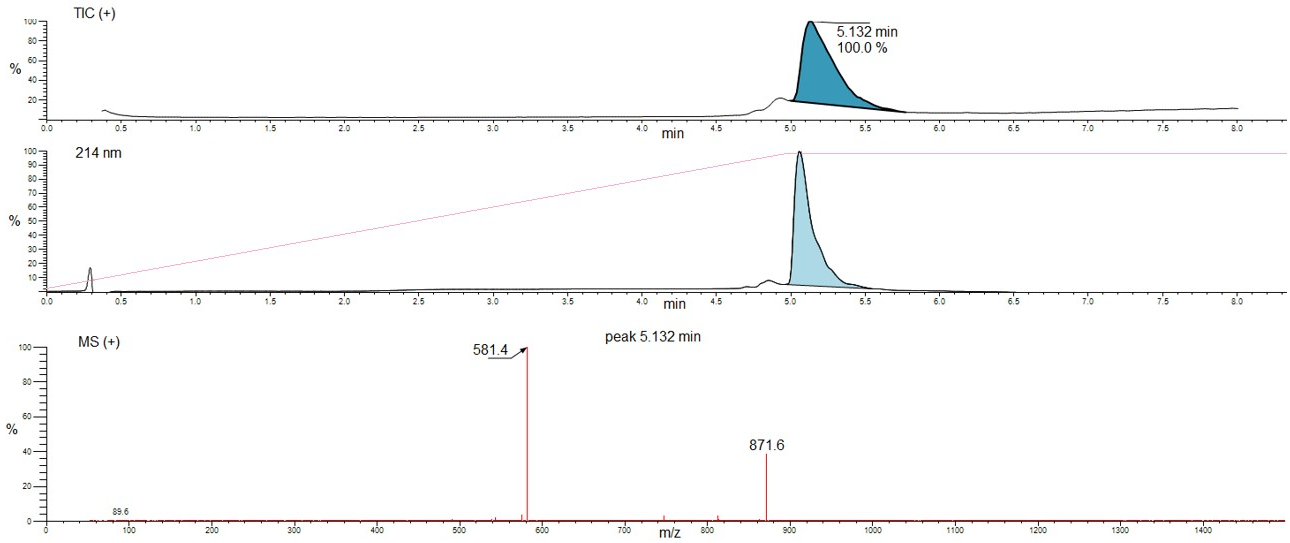

Figure S13. Total ion count chromatogram (TIC+) and mass spectral data for compound **NVFRET** after cleavage of the assembled peptide from SPPS resin and HPLC purification. The solvent gradient (%B = acetonitrile) is highlighted in pink in the DAD chromatogram at 214nm.

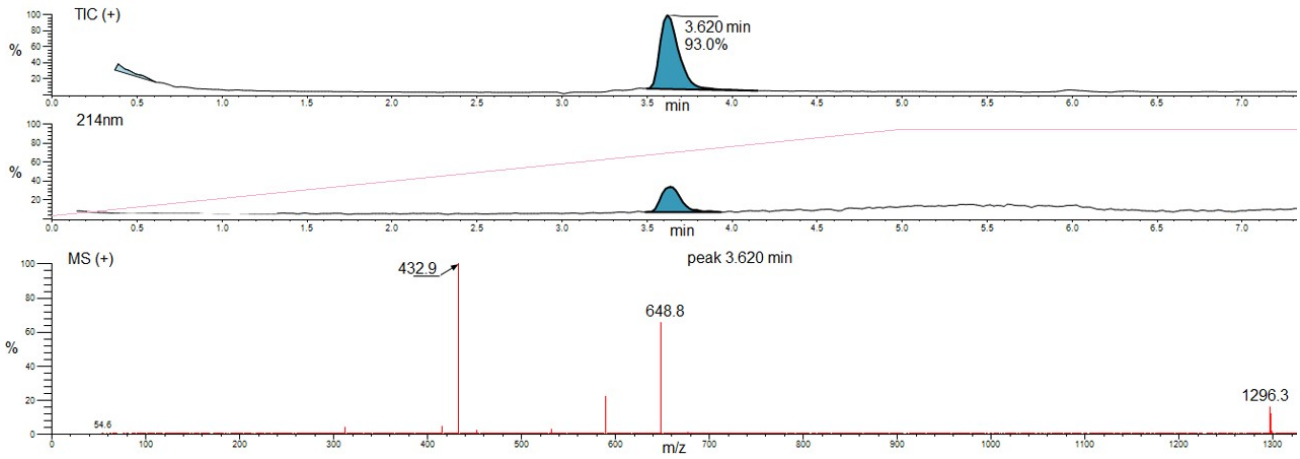

Figure S14. Total ion count chromatogram (TIC+) and mass spectral data for compound **NPFRET** after cleavage of the assembled peptide from SPPS resin and HPLC purification. The solvent gradient (%B = acetonitrile) is highlighted in pink in the DAD chromatogram at 214nm.

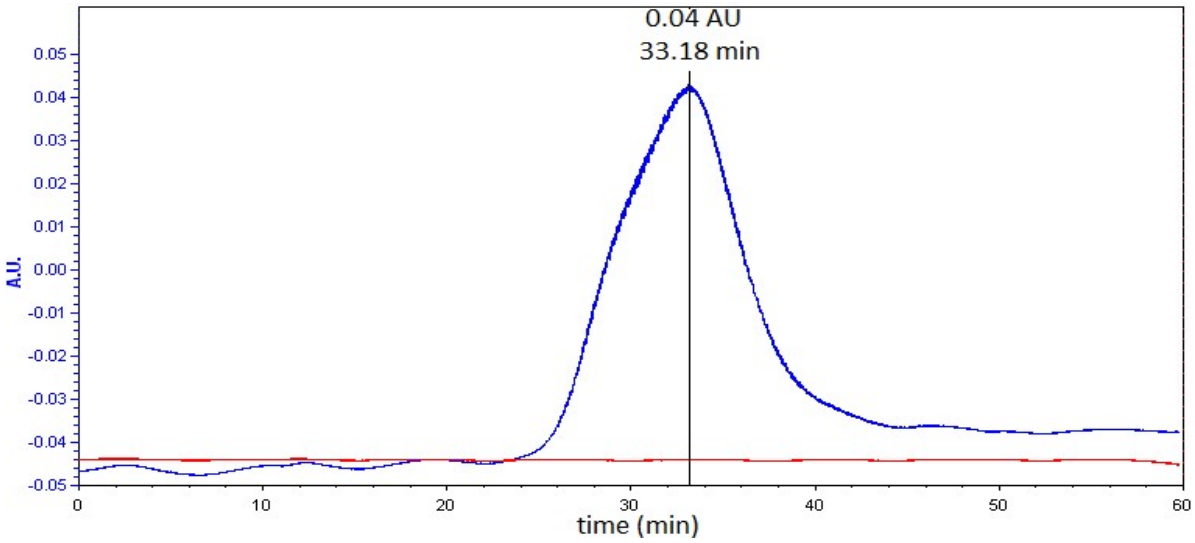

Gel filtration chromatogram (Sephadex G-15, 1 mL/min, 20 mM Bis-Tris, 150 mM NaCl, 1 mM DTT, 1 mM EDTA, pH 7.8, 0.02% Tween) of FIPV-M^{pro}

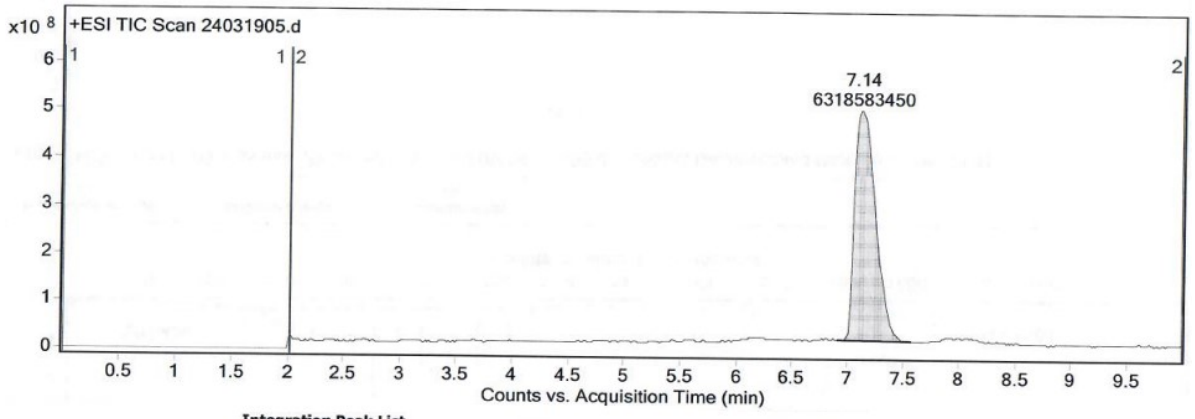

Integration Peak List

Peak	Start	RT	End	Height	Area	Area %
1	6.91	7.14	7.58	479186990	6318583450	100

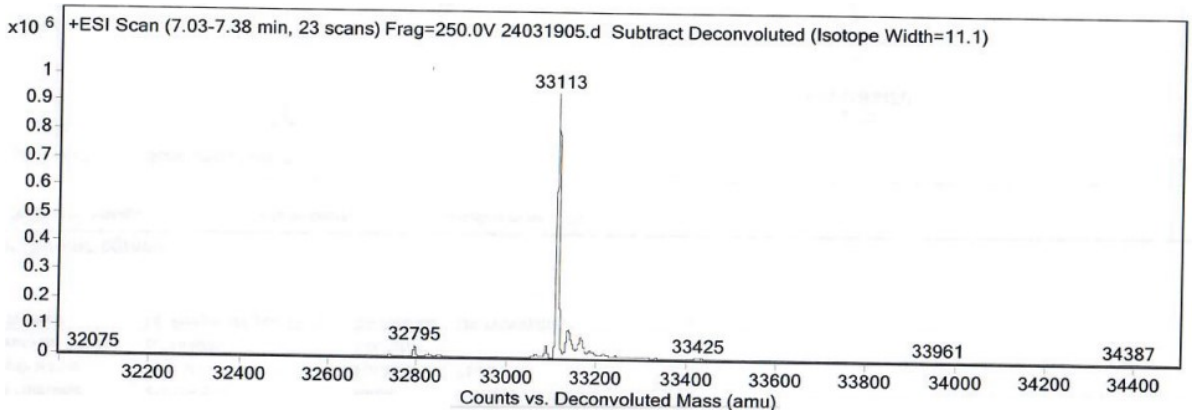

Chromatogram and deconvoluted mass spectrum of FIPV-M^{pro}

Figure S15. Chromatographic and ESI mass-spectrometric characterization of FIPV-M^{pro}.

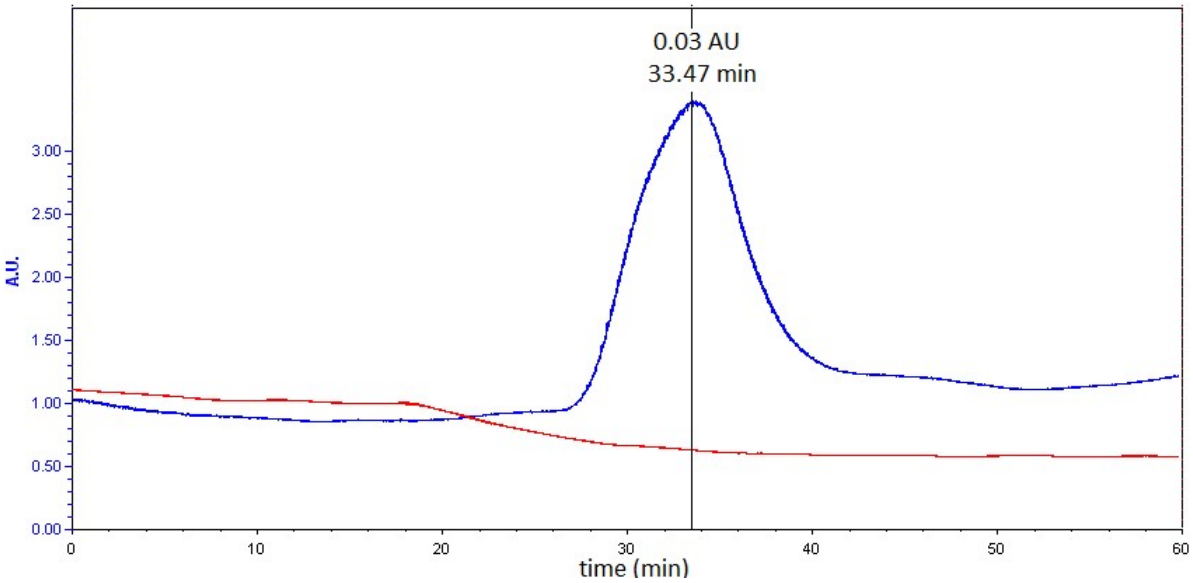

Gel filtration chromatogram (Sephadex G-15, 1 mL/min, 20 mM Bis-Tris, 150 mM NaCl, 1 mM DTT, 1 mM EDTA, pH 7.8, 0.02% Tween) of PEDV-M^{pro}.

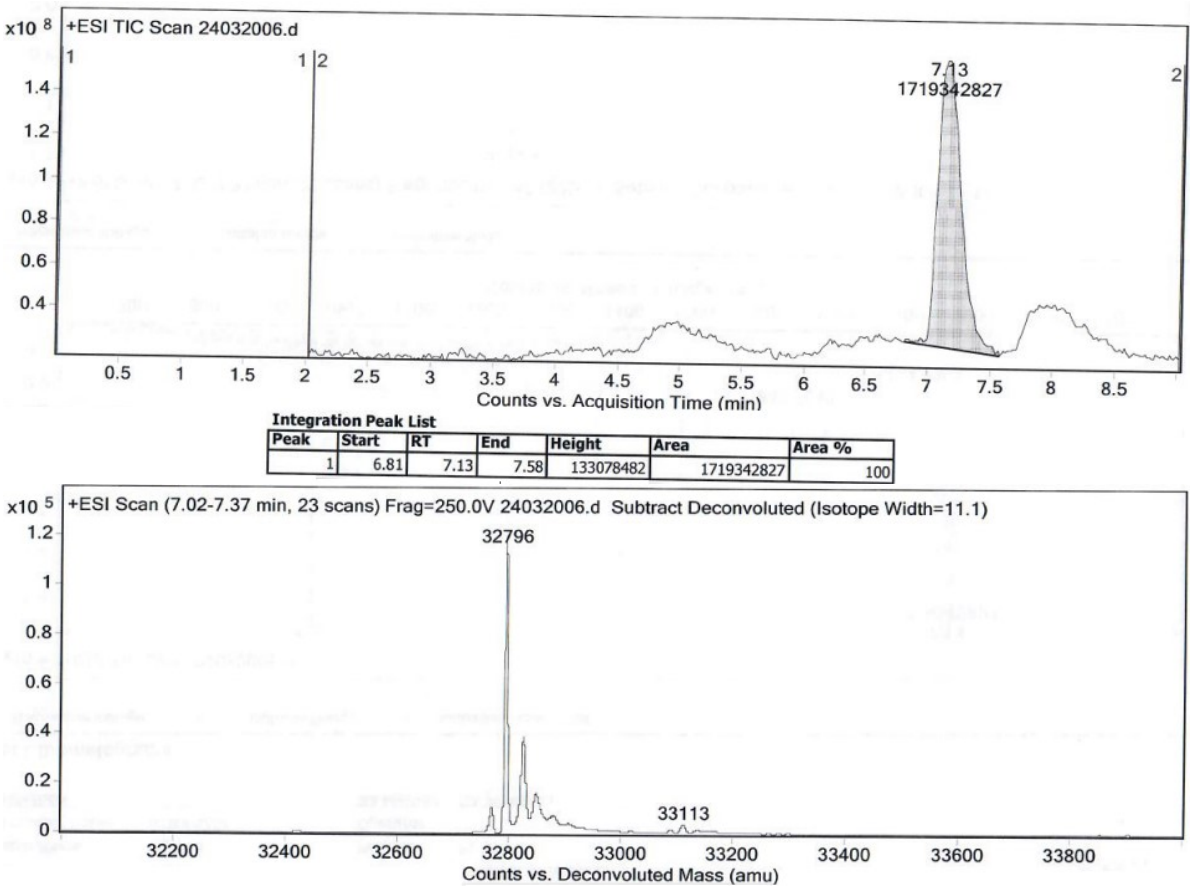

Chromatogram and deconvoluted mass spectrum of PEDV-M^{pro}.

Figure S16. Chromatographic and ESI mass-spectrometric characterization of PEDV-M^{pro}.

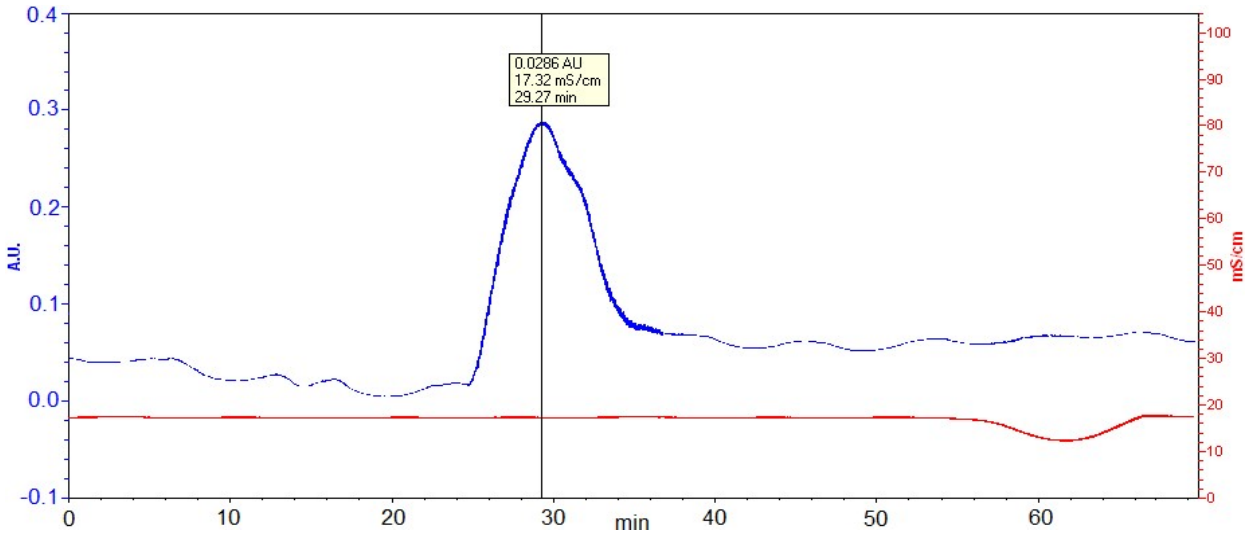

Gel filtration chromatogram (Sephadex G-15, 1 mL/min, 20 mM Bis-Tris, 150 mM NaCl, 1 mM DTT, 1 mM EDTA, pH 7.8, 0.02% Tween) of EqCoV-M^{pro}.

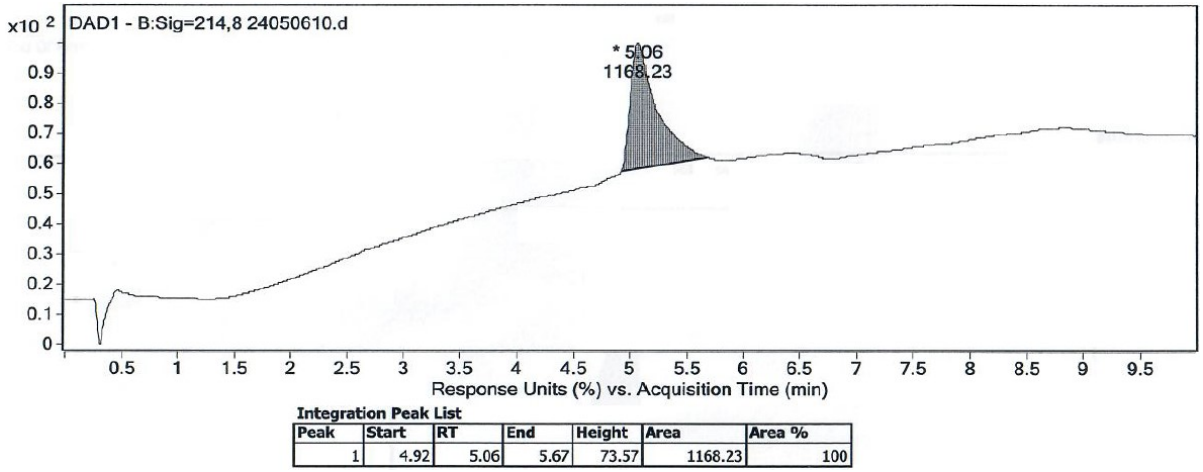

Integration Peak List

Peak	Start	RT	End	Height	Area	Area %
1	4.92	5.06	5.67	73.57	1168.23	100

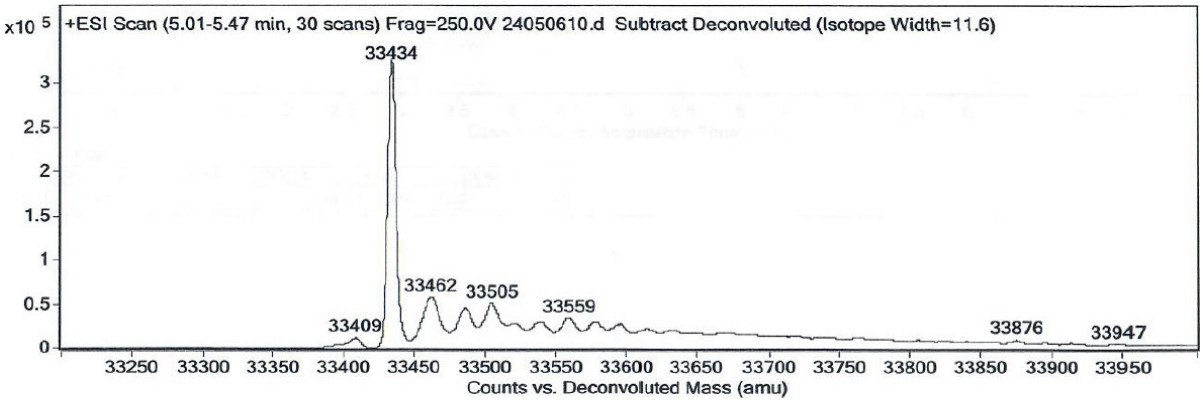

Chromatogram and deconvoluted mass spectrum of EqCoV-M^{pro}.

Figure S17. Chromatographic and ESI mass-spectrometric characterization of EqCoV-M^{pro}.

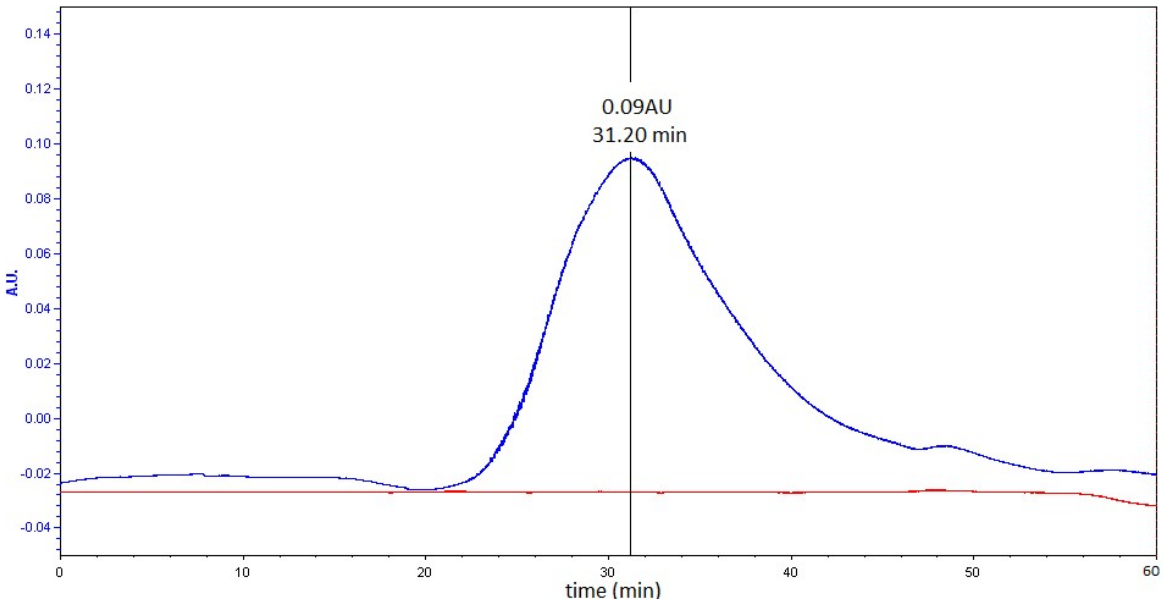

Gel filtration chromatogram (Sephadex G-15, 1 mL/min, 20 mM Bis-Tris, 150 mM NaCl, 1 mM DTT, 1 mM EDTA, pH 7.8, 0.02% Tween) of HRV-M^{pro}

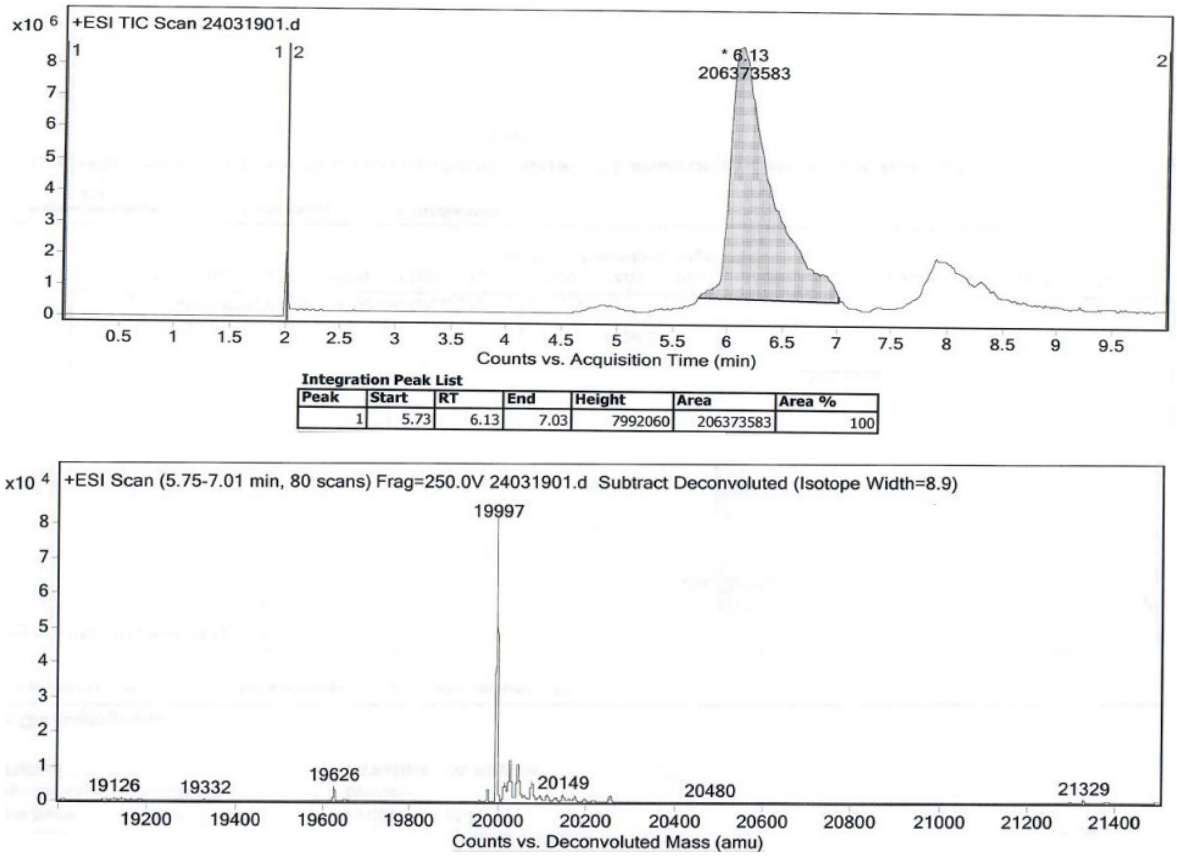

Chromatogram and deconvoluted mass spectrum of HRV-M^{pro}

Figure S18. Chromatographic and ESI mass-spectrometric characterization of HRV-M^{pro}.

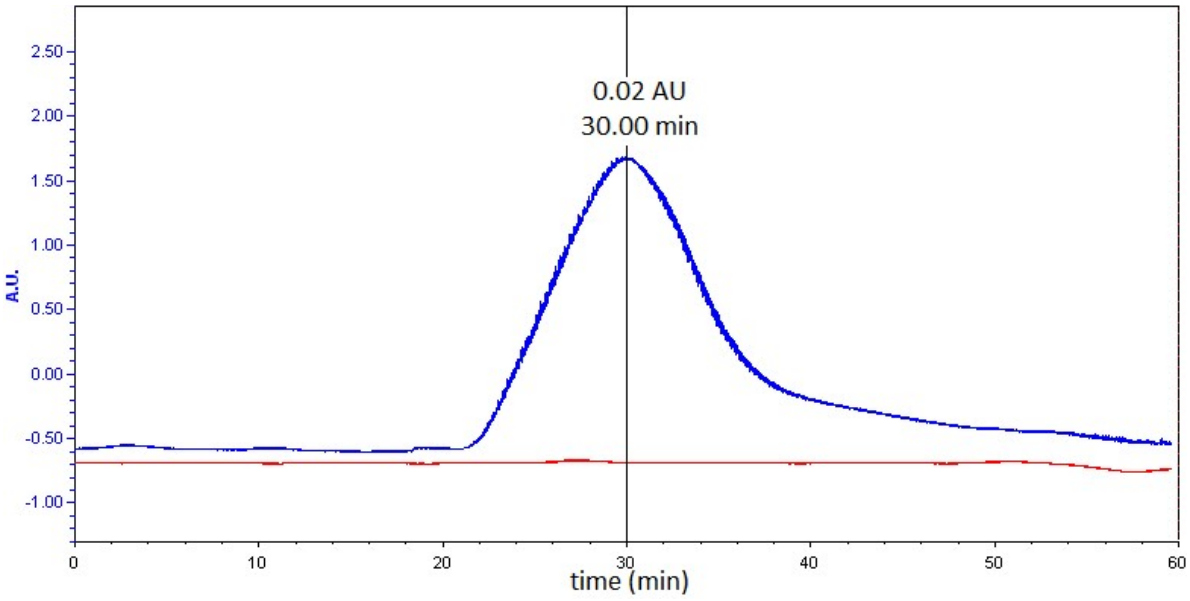

Gel filtration chromatogram (Sephadex G-15, 1 mL/min, 20 mM Bis-Tris, 150 mM NaCl, 1 mM DTT, 1 mM EDTA, pH 7.8, 0.02% Tween) of PV-M^{pro}

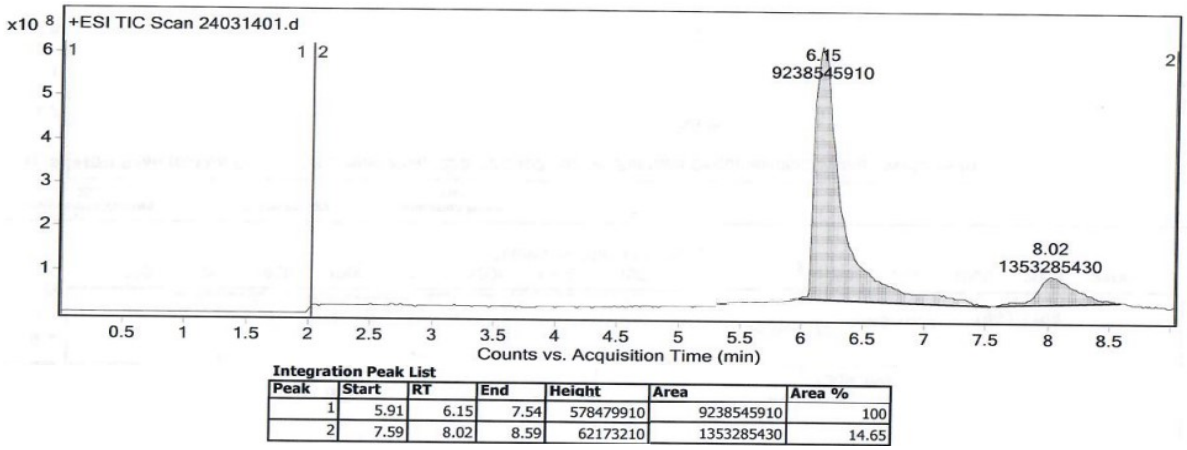

Integration Peak List

Peak	Start	RT	End	Height	Area	Area %
1	5.91	6.15	7.54	578479910	9238545910	100
2	7.59	8.02	8.59	62173210	1353285430	14.65

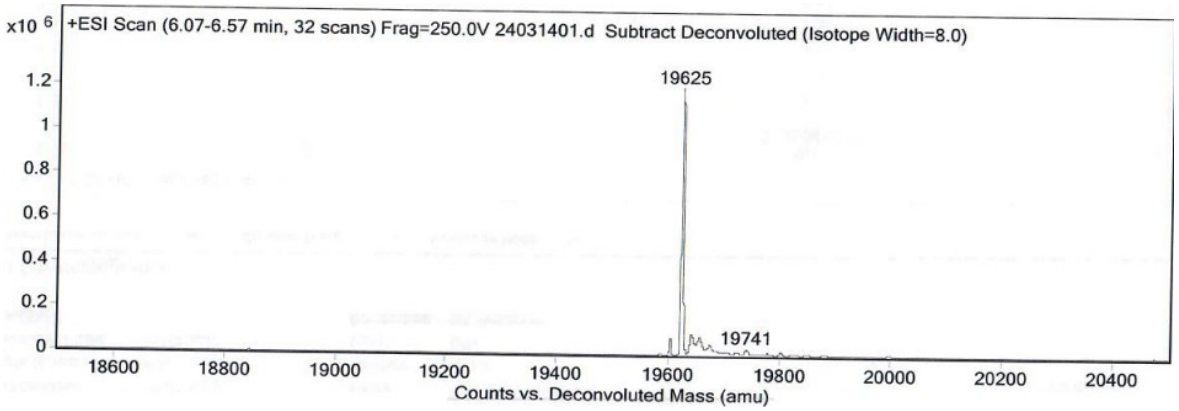

Chromatogram and deconvoluted mass spectrum of PV-M^{pro}

Figure S19. Chromatographic and ESI mass-spectrometric characterization of PV-M^{pro}.

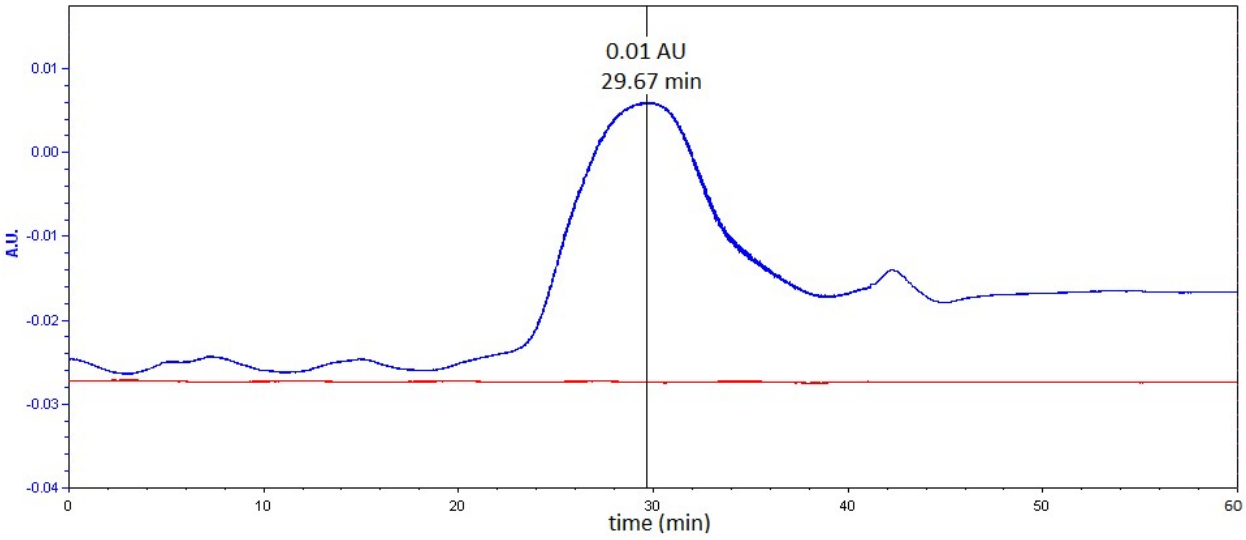

Gel filtration chromatogram (Sephadex G-15, 1 mL/min, 20 mM Bis-Tris, 150 mM NaCl, 1 mM DTT, 1 mM EDTA, pH 7.8, 0.02% Tween) of EV71-M^{pro}

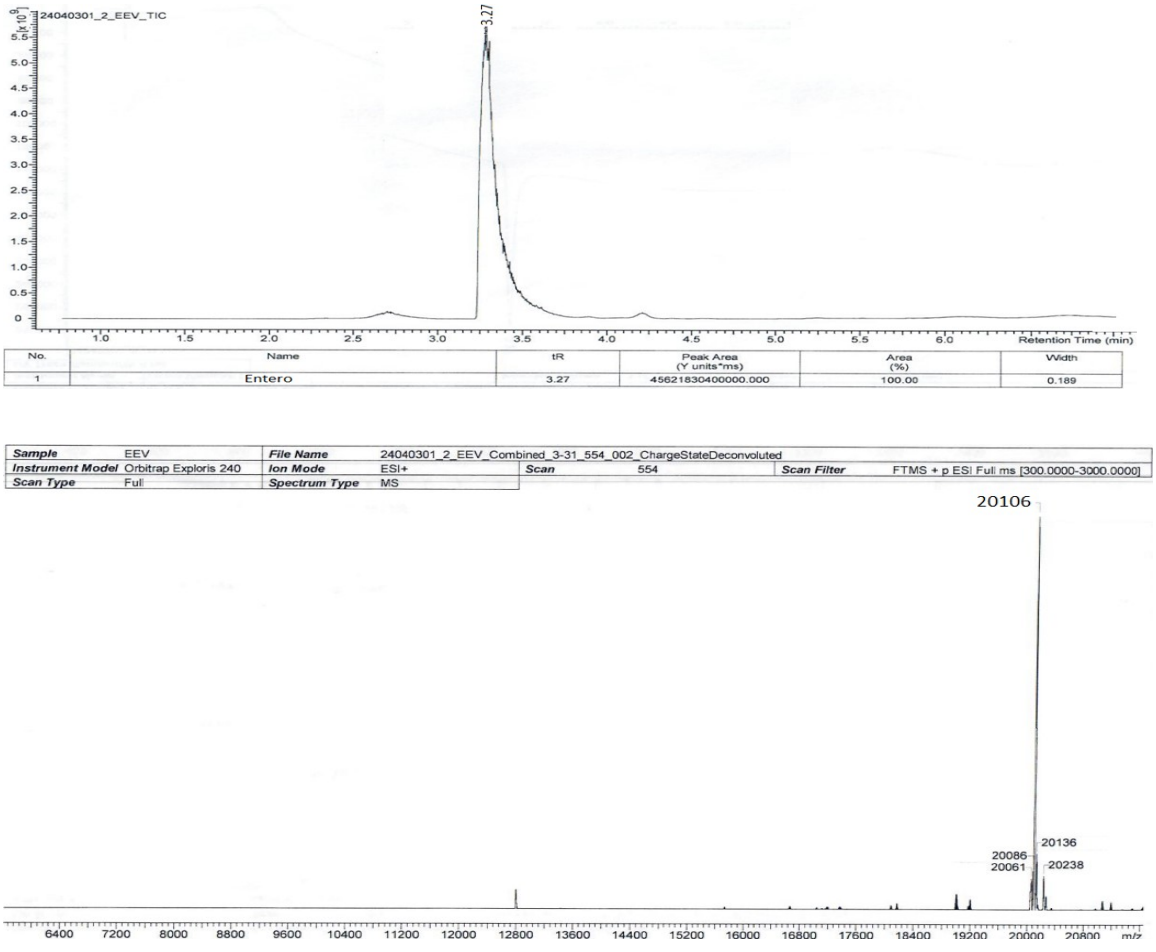

Chromatogram and deconvoluted mass spectrum of EV71-M^{pro}

Figure S20. Chromatographic and ESI mass-spectrometric characterization of EV71-M^{pro}.

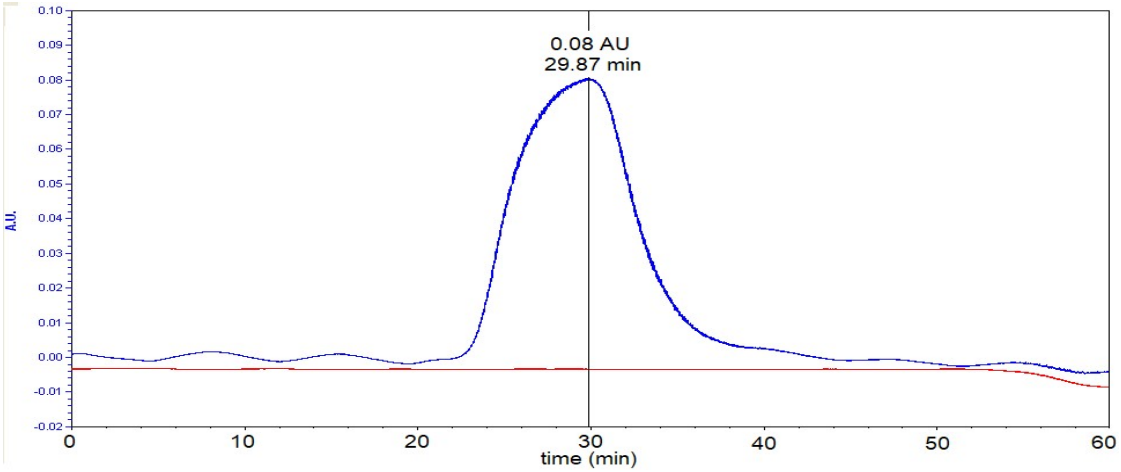

Gel filtration chromatogram (Sephadex G-15, 1 mL/min, 20 mM Bis-Tris, 150 mM NaCl, 1 mM DTT, 1 mM EDTA, pH 7.8, 0.02% Tween) of NV-M^{pro}

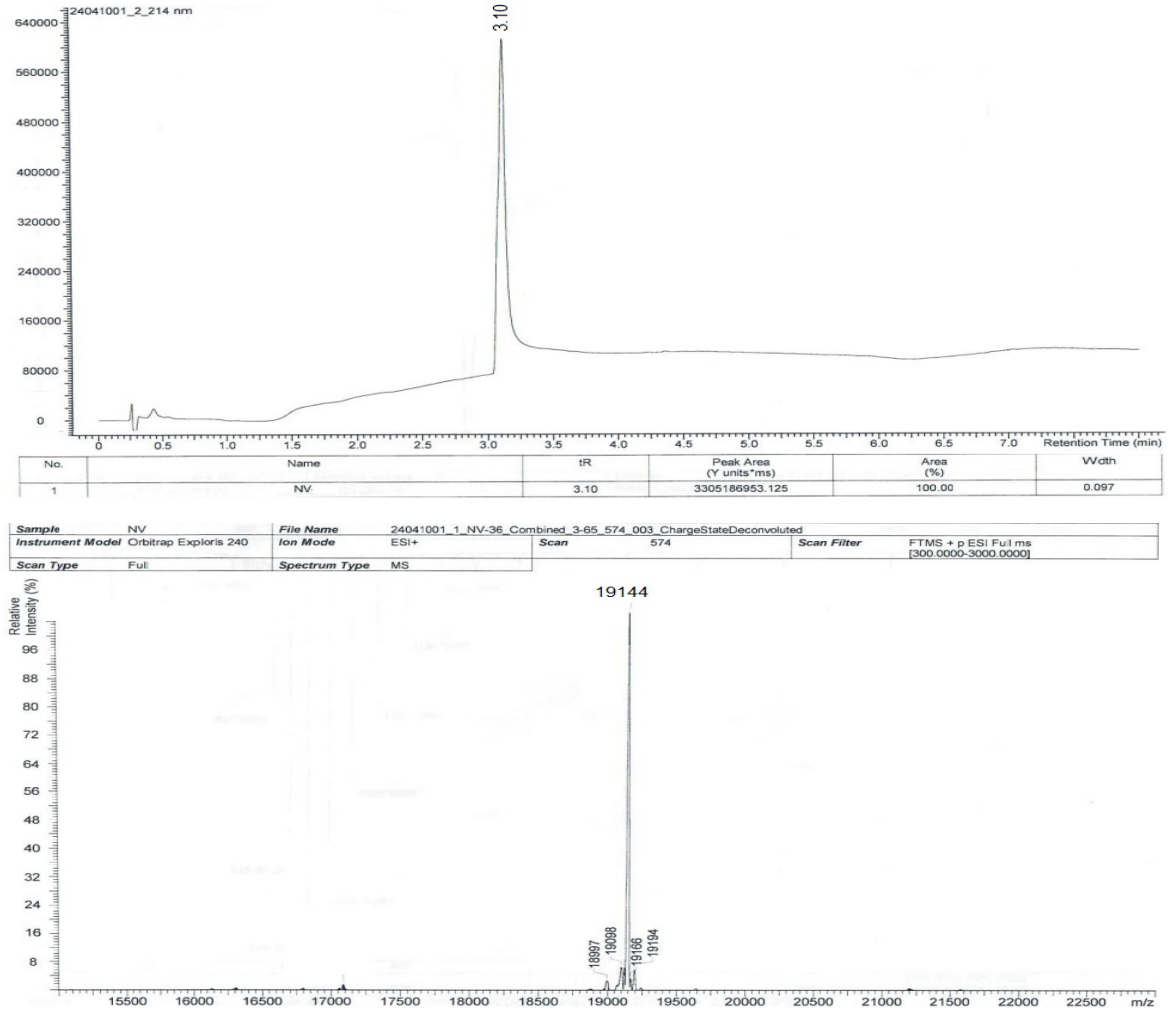

Chromatogram and deconvoluted mass spectrum of NV-M^{pro}

Figure S21. Chromatographic and ESI mass-spectrometric characterization of NV-M^{pro}.

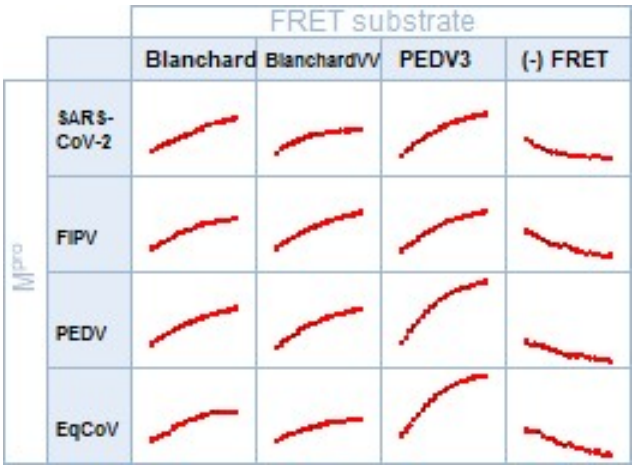

Figure S22. Reaction progression curves of various M^{pro}s with selected FRET substrates. The curves depict fluorescence released over the course of a 10 min assay.

Blanchard: **2-AbzSVTLQ↓SGY$^{(NO2)}$R** —SARS-CoV-2 M^{pro}→ **2-AbzSVTLQ** + **SGY$^{(NO2)}$R**

1174 g/mol 666 g/mol 526 g/mol

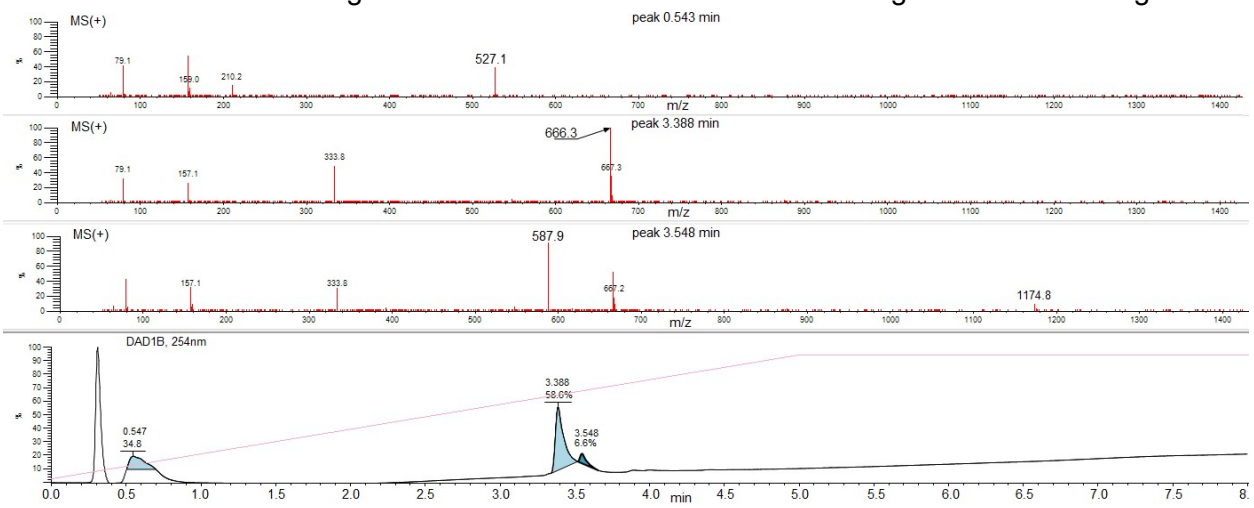

PEDV3: 2-AbzSTLQ↓SGY$^{(NO2)}$R —SARS-CoV-2 M^{pro}→ **2-AbzSTLQ** + **SGY$^{(NO2)}$R**

1075 g/mol 566 g/mol 526 g/mol

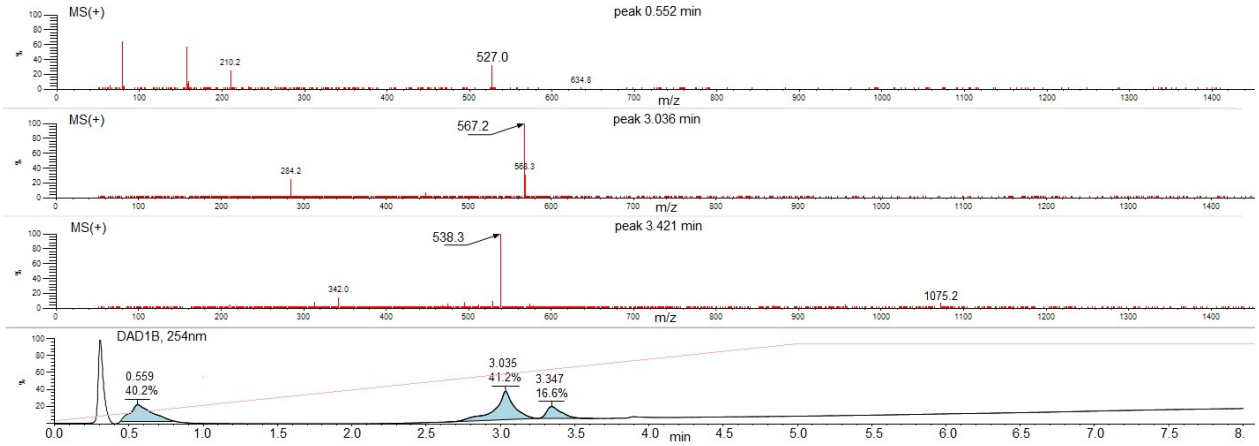

(-) FRET: 2-AbzSTLAAGY$^{(NO2)}$R —SARS-CoV-2 M^{pro}→ no cleavage

1002 g/mol

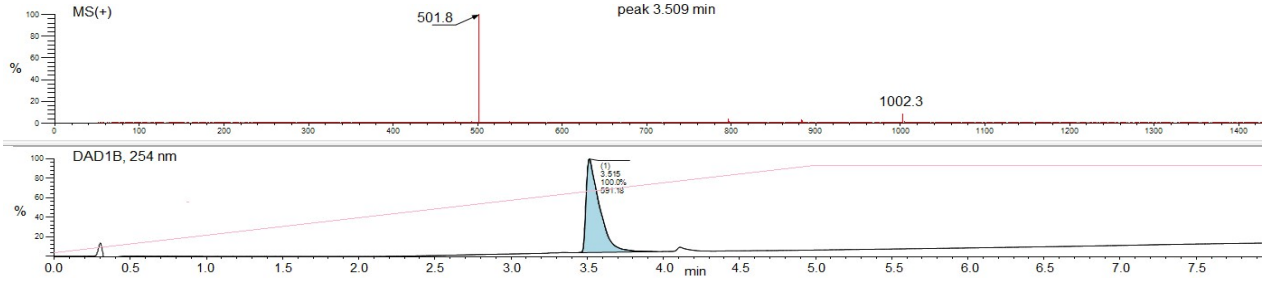

Figure S23. LCMS analysis of cleavage products formed by reaction of Blanchard FRET (top) and PEDV3 FRET (middle) and negative control ((-)FRET, bottom) with SARS-CoV-2 M^{pro} after 10 min cleavage highlighting cleavage specificity of the main protease.

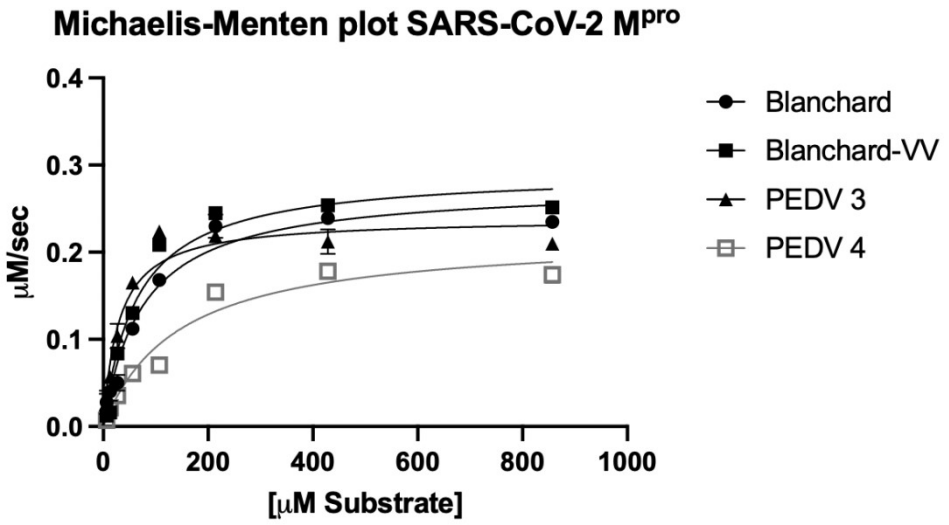

	Blanchard	Blanchard-VV	PEDV 3	PEDV 4
v_{max}, µM s^{-1}	0.2763±0.02	0.2927±0.02	0.2386±0.04	0.2201±0.03
K_M, µM	82±14	64±10	30±8	142±18
Goodness of fit				
R squared	0.9664	0.9619	0.9321	0.9545

Figure S24. Michaelis-Menten plot of various coronavirus FRETs with SARS-CoV-2 M^{pro}.

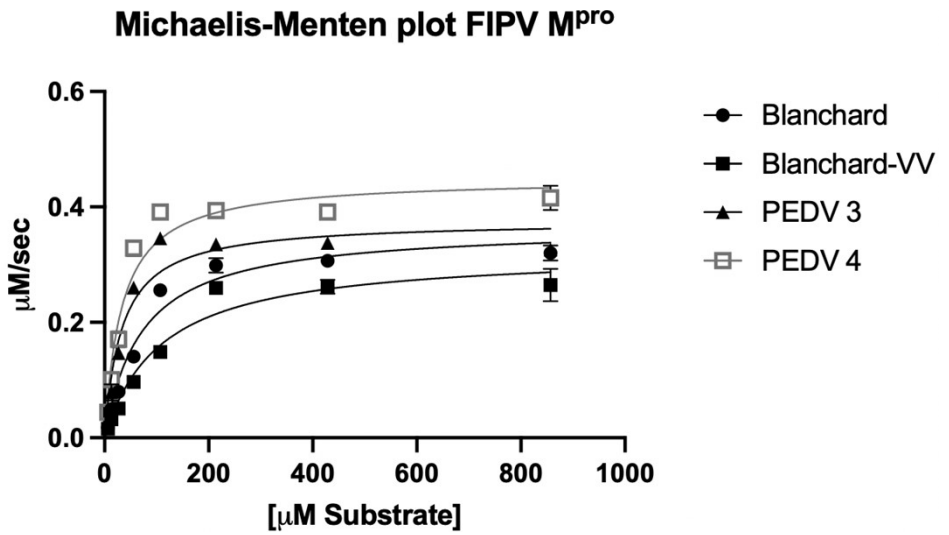

	Blanchard	Blanchard-VV	PEDV 3	PEDV 4
v_{max}, µM s^{-1}	0.3661±0.03	0.3231±0.04	0.3762±0.04	0.4199±0.04
K_M, µM	72±12	85±15	33.1±12	32.9±11
Goodness of fit				
R squared	0.9675	0.9556	0.9322	0.9471

Figure S25. Michaelis-Menten plot of various coronavirus FRETs with FIPV M^{pro}.

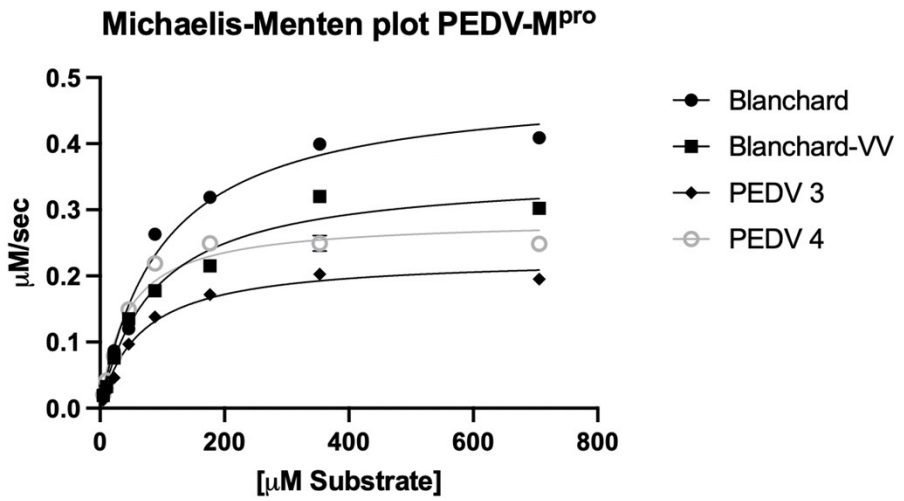

	Blanchard	Blanchard-VV	PEDV 3	PEDV 4
v_{max}, µM s^{-1}	0.489±0.03	0.360±0.04	0.269±0.03	0.228±0.01
K_M, µM	100±18	85±10	38±11	65±12
Goodness of fit				
R squared	0.9817	0.9801	0.9713	0.9892

Figure S26. Michaelis-Menten plot of various coronavirus FRETs with PEDV M^{pro} .

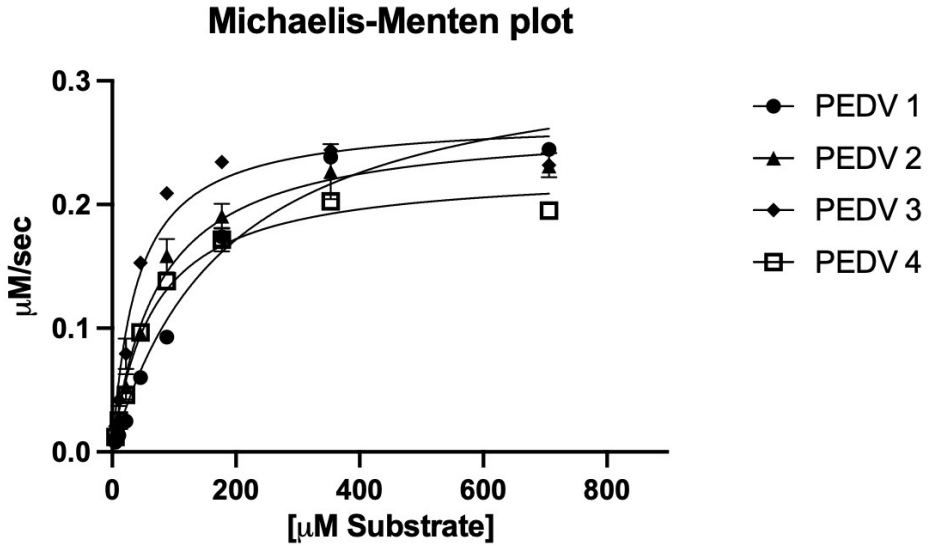

	PEDV 1	PEDV 2	PEDV 3	PEDV 4
v_{max}, µM s^{-1}	0.330±0.02	0.266±0.02	0.269±0.03	0.248±0.01
K_M, µM	192±26	63±11	38±11	65±12
Goodness of fit				
R squared	0.9852	0.9819	0.9713	0.9892

Figure S27. Michaelis-Menten plot of various PEDV FRETs with PEDV M^{pro}.

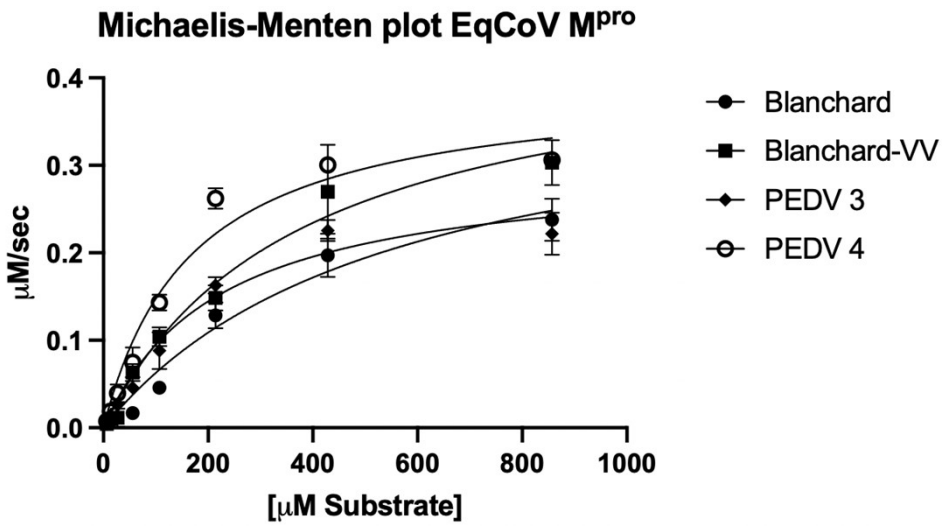

	PEDV 1	PEDV 2	PEDV 3	PEDV 4
v_{max}, µM s^{-1}	0.4075	0.4516	0.3027	0.3963
K_M, µM	549.1	371.1	219.1	168.5
Goodness of fit				
R squared	0.9632	0.9630	0.9623	0.9664

Figure S28. Michaelis-Menten plot of various coronavirus FRETs with EqCoV M^{pro}.

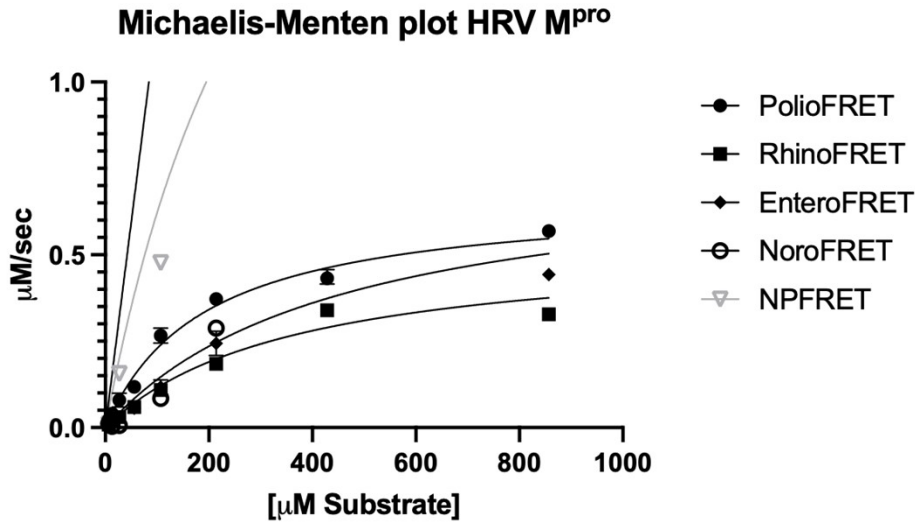

	PVFRET	HRVFRET	EVFRET	NVFRET	NPFRET
v_{max}, µM s^{-1}	0.6694±0.06	0.5348±0.08	0.7709±0.08	n.d.*	n.d.*
K_M, µM	192.1±35	363.0±83	455.3±112	n.d.*	n.d.*
Goodness of fit					
R squared	0.9836	0.9593	0.9554	0.8414	0.07005

Figure S29. Michaelis-Menten plot of various picornavirus FRETs with HRV M^{pro}. No exact data for entries with (*) could be determined due lack of convergence.

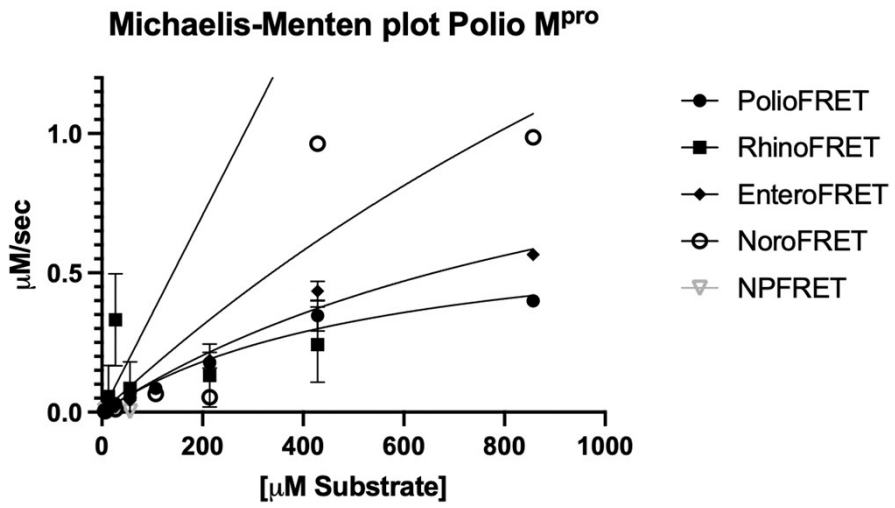

	PVFRET	HRVFRET	EVFRET	NVFRET	NPFRET
v_{max}, μM s^{-1}	0.6969±0.06	n.d.*	1.366±0.30	4.136±1.36	n.d.*
K_M, μM	569.3±95	n.d.*	1143±205	2452±830	1386
Goodness of fit					
R squared	0.9693	0.7278	0.9756	0.8315	0.7265

Figure S30. Michaelis-Menten plot of various picornavirus FRETs with PV M^{pro}. No exact data for entries with (*) could be determined due lack of convergence.

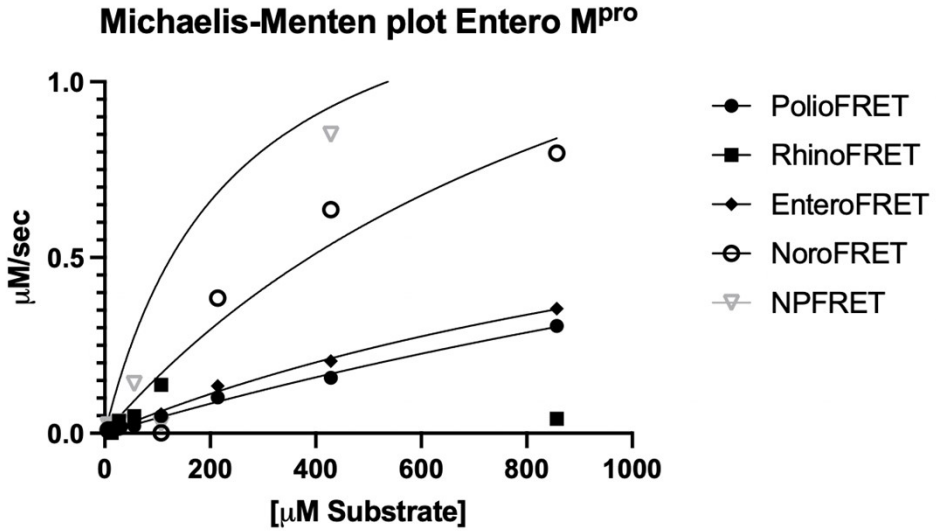

	PVFRET	HRVFRET	EVFRET	NVFRET	NPFRET
v_{max}, μM s^{-1}	1.442±0.21	n.d.*	1.029±0.13	1.914±0.29	n.d.*
K_M, μM	3223	237.1	1641	1097	n.d.*
Goodness of fit					
R squared	0.9956	0.2027	0.9957	0.9246	0.04465

Figure S31. Michaelis-Menten plot of various picornavirus FRETs with EV71 M^{pro}. No exact data for entries with (*) could be determined due lack of convergence.

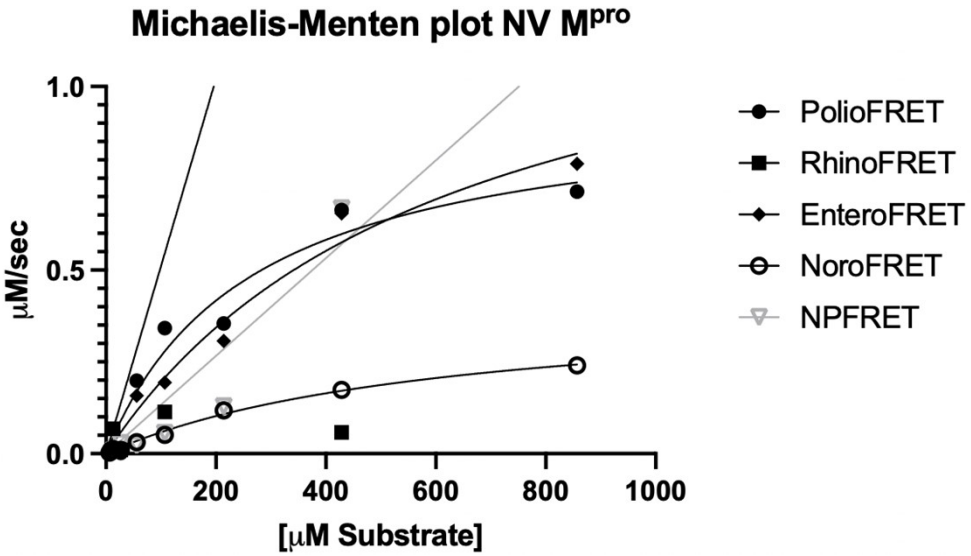

	PVFRET	HRVFRET	EVFRET	NVFRET	NPFRET
v_{max}, µM s^{-1}	0.9659±0.10	n.d.*	1.410±0.16	0.4163±0.08	n.d.*
K_M, µM	263.5	n.d.*	621.5	613.0	n.d.*
Goodness of fit					
R squared	0.9565	0.7016	0.9735	0.9945	0.9643

Figure S32. Michaelis-Menten plot of various picornavirus FRETs with NV M^{pro} . No exact data for entries with (*) could be determined due lack of convergence.

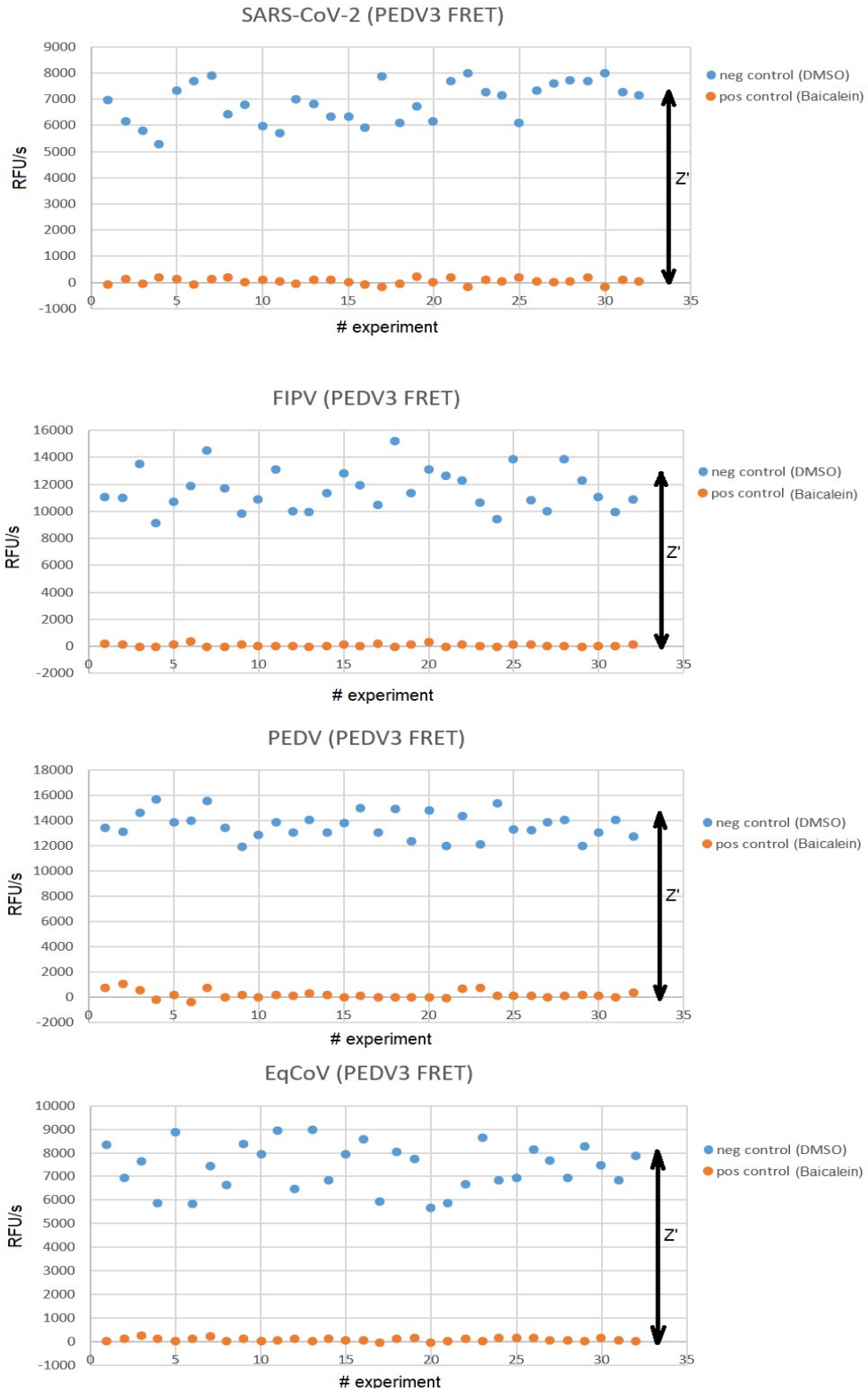

Figure S33. Z' assay quality statistics for different coronavirus M^{pro}s (100 nM) with PEDV 3 FRET substrate (10 μM). Samples were prepared with 50 μM baicalein (positive control) or 50 μM DMSO (negative control) and repeated in duplicate for *n*=32.